J. Fluid Mech. (2007), *vol.* 571, *pp.* 177–189.
doi:10.1017/S0022112006002862 Printed in the United Kingdom

The effect of buoyancy on vortex breakdown in a swirling jet

By DINA MOURTAZIN AND JACOB COHEN

Faculty of Aerospace Engineering, Technion – IIT, Haifa, 32000, Israel

(Received 17 March 2006 and in revised form 6 August 2006)

The purpose of this experimental study is to explore the effect of buoyancy on vortex breakdown (VB) in swirling jets. Three non-dimensional parameters govern the flow: the jet exit Reynolds number, the swirl ratio and the Richardson number (buoyancy). The experimental apparatus consists of a vertical swirling water jet which discharges into a large tank. Moderate values of the Reynolds number are used, in the range $150 \leqslant Re \leqslant 600$. Swirl is imparted to the jet in a rotating chamber whereas the temperature difference between the jet and its surroundings is established by passing the jet through a heat exchanger, immersed in a circulating water bath with a controlled temperature. Vector maps of the vertical mid-plane and horizontal cross-sections are obtained by particle image velocimetry (PIV) measurements. It is demonstrated that VB can be effectively suppressed (enhanced) when there is a negative (positive) temperature difference between the jet core and its surrounding fluid. The experimental critical swirl ratio for the appearance of VB is found to be in good agreement with a simple criterion, originally derived by Billant, Chomaz & Huerre (J. Fluid Mech., vol. 376, 1998, p. 183) for isothermal swirling jets and extended here to include buoyancy effects. The transition of VB from a closed bubble to an open cone configuration is mapped in terms of the Reynolds and Richardson numbers. Finally, the effect of the upstream velocity field on the critical rotation rate for the onset of VB and its configuration is exhibited using two different interchangeable rotating chambers.

1. Introduction

Vortex breakdown (VB) is a remarkable phenomenon which may occur in swirling flows. It is characterized by a sudden deceleration of the flow near the axis and the formation of a stagnation point accompanied by the divergence of the stream surface. Downstream of the stagnation point a region of reverse flow forms and the wake of the expanded vortical structure may undergo large-scale velocity fluctuations. As such VB can have either detrimental effects, for example over delta wings at high angle of attack, or beneficial ones, such as a flame stabilizer utilizing the fast spreading and rapid mixing of the incoming flow with its surroundings. Thus there is a need for better understanding of the phenomenon in order to either prevent the breakdown or promote it. In isothermal flows VB occurs when the ratio between the swirling and axial velocities exceeds a certain value of order unity. The inclusion of buoyancy effects in swirling jets can result in the increase or decrease of this ratio, i.e. providing possible VB control.

Thermal effects on axisymmetric VB have been reported in various flow configurations. Arkadyev *et al.* (1993) examined these effects numerically in fluid

contained within a rotating concentric spherical annulus. Their results show that the flow field characteristics depend on the relative strength of the imposed temperature difference and the rotation rate, and that for certain conditions a ring-type VB may appear (in addition to the bubble type). Several numerical studies have been carried out in a cylindrical container with a rotating endwall. Lugt & Abboud (1987) used a Boussinesq fluid, with the temperature at the bottom stationary endwall disk higher than that at the top rotating disk (unstable stratification). Their results show that the occurrence and properties of the stagnation bubble are strongly influenced by buoyancy. For a similar setup but in a stably stratified flow it was found (Kim & Hyun 1997; Lee & Hyun 1999) that when the appropriate Richardson number is greater than order unity, the separation bubble disappears. More recently, Herrada & Shtern (2003*a*, *b*) carried out numerical simulations of a compressible flow in a sealed cylinder with a rotating bottom disk, and showed that a positive (negative) axial temperature gradient along the downward flow can diminish (enlarge) the VB bubble and therefore suppress (enforce) VB.

Isothermal swirling jets have a relatively simple geometry and are primarily governed by a single parameter (the swirl ratio). Nevertheless, the resulting flow field as a function of the swirl ratio is rich and complex and therefore has recently attracted many theoretical and numerical studies providing similarity solutions (Shtern, Hussain & Herrada 2000), analysing the relative importance and the interaction between Kelvin–Helmholtz and centrifugal instabilities (e.g. Martin & Meiburg 1994; Sun *et al.* 2002; Gallaire & Chomaz 2003*a*) and trying to identify the transition from convective to absolute instability and its relation to the onset of VB (e.g. Lim & Redekopp 1998; Loiseleux, Delbende & Huerre 2000; Gallaire & Chomaz 2003*b*; Ruith *et al.* 2003; Gallaire *et al.* 2006). Several experimental investigations have been carried out to characterize the stability of a swirling jet in pre-breakdown conditions (Loiseleux & Chomaz 2002), the influence of the upstream velocity field (Ivanic, Foucault & Pecheux 2003), the conditions for VB and its various forms (Billant, Chomaz & Huerre 1998), the robustness of VB to azimuthal forcing at the nozzle periphery (Gallaire, Rott & Chomaz 2004) which may be explained by the core mechanism leading to VB (Wang & Rusak 1977), and the stability of a swirling jet in general and the relation of VB to the existence of self-excited/globally unstable modes in particular (Liang & Maxworthy 2005).

The aim of the present study is to reveal the effect of buoyancy on the onset and forms of VB in swirling jets. We first extend the simple VB criterion derived and experimentally verified by Billant *et al.* (1998) for an isothermal swirling jet, to include thermal effects due to lateral temperature gradients. We then verify this criterion experimentally and relate the final configuration of the VB to its position in a Reynolds–Richardson map.

2. A simple vortex breakdown criterion including buoyancy effects

In this section the simple necessary criterion for the onset of vortex breakdown, derived by Billant *et al.* (1998, hereinafter referred to as BCH), in the same spirit as the first stage of Escudier & Keller's (1983) theory, is extended to include buoyancy effects. Accordingly, a free vortex undergoing conical breakdown in a jet of infinite extent (figure 1) is considered. The cylindrical coordinate system is used (x, r, θ), where x and r are the axial and radial distances and θ is the azimuthal angle. The corresponding velocity components are (V_x, V_r, V_θ). The flow is assumed to be steady and laminar. Viscous, diffusive and entrainment effects are supposed to be negligible.

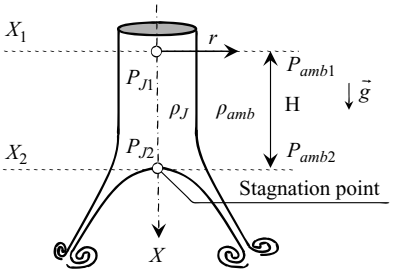

FIGURE 1. Schematic drawing of cone vortex breakdown.

Applying the Bernoulli equation between two cross-stream planes, X_1 (far upstream of the stagnation point) and X_2 (the plane containing the stagnation point), along the centreline, and away from it where the ambient fluid is at rest, respectively yields

$$P_{J_1} + \rho_J g H + 0.5\rho_J V_x^2(X_1, 0) = P_{J_2}, \tag{2.1}$$

$$P_{amb_2} = P_{amb_1} + \rho_{amb} g H, \tag{2.2}$$

where P is the pressure, ρ is the fluid density, g is the acceleration due to gravity and $H = X_2 - X_1$ is the vertical distance between the two planes. The subscripts J and amb correspond respectively, to the jet and ambient fluid properties, whereas the subscripts 1 and 2 indicate the associated cross-stream planes. At the X_1-plane the radial pressure gradient is balanced by the centrifugal force

$$P_{amb_1} = P_{J_1} + \int_0^\infty \rho_J \frac{V_\theta^2(r, X_1)}{r}\, \mathrm{d}r. \tag{2.3}$$

It should be noted that as the radial distance in (2.3) approaches the ambient fluid, the associated integrand becomes approximately zero. The radial density variation due to the temperature difference between the ambient fluid and the jet ($\Delta T = T_J - T_{amb}$) is approximated as

$$\rho_{amb} \approx \rho_J - \frac{\partial \rho}{\partial T}\Delta T = \rho_J(1 + \beta \Delta T), \qquad \beta = -\frac{1}{\rho_J}\frac{\partial \rho}{\partial T}, \tag{2.4}$$

where β is the coefficient of thermal expansion.

As the cone is open to the surrounding fluid and the flow is almost at rest, it is assumed that $P_{J_2} = P_{amb_2}$. Finally, substituting (2.2)–(2.4) into (2.1) leads to the following necessary condition for a vortex breakdown (VB_{crit}):

$$VB_{crit} = \frac{1}{V_x^2(X_1, 0)} \int_0^\infty \frac{V_\theta^2}{r}\, \mathrm{d}r + \frac{gH\beta\Delta T}{V_x^2(X_1, 0)} \equiv S_{int} + Ri \geqslant \frac{1}{2}, \tag{2.5}$$

where S_{int} and Ri are the swirl integral and the Richardson number (buoyancy effect), respectively. The inequality sign is applied to a bubble vortex breakdown configuration in which the stagnant zone is separated from the ambient quiescent fluid. In § 4.1, this criterion is verified by experimental results.

3. Experimental setup and procedures

3.1. *Apparatus*

A schematic view (drawn to scale) of the experimental apparatus, consisting of a vertical swirling jet discharging into a large transparent cylindrical tank, is shown

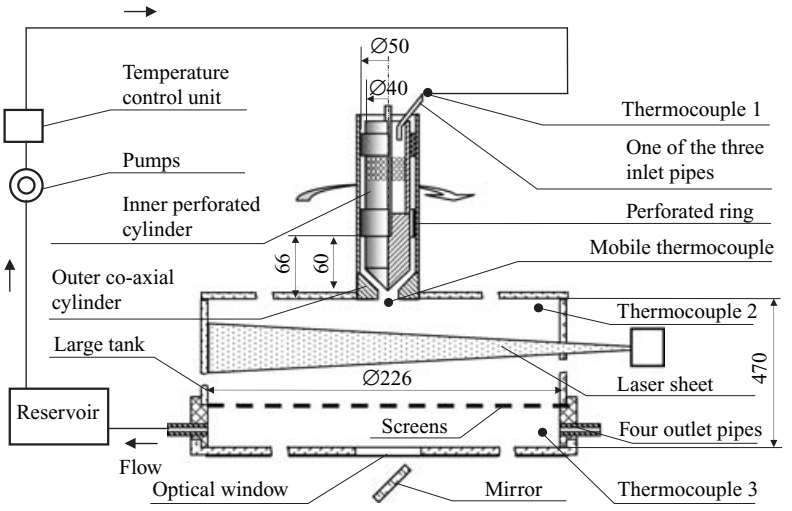

FIGURE 2. Schematic view of experimental apparatus.

in figure 2. After exiting the tank, the water circulates through a temperature control unit and returns to the rotating chamber. Water circulation through the system is maintained by two piston-type metering pumps driven by a single control motor.

Three parameters govern the flow: the flow rate (Q), the angular momentum of the fluid and the temperature difference between the jet and the ambient fluid. These respectively correspond to the non-dimensional jet exit Reynolds number ($Re = 4Q/(\pi D\nu)$, where D is the inner diameter of the nozzle at the exit plane and ν the kinematic viscosity of water at room temperature), the swirl ratio (S_{int}) and the Richardson number (Ri). The definitions of the latter two are given in (2.5). The flow rate (jet axial velocity) is maintained with a DC motor controller and monitored by an optical tachometer. To reduce pulsations, the pumps are set 180° out of phase with each other, two 2 l reservoirs with flexible tubing in the system are utilized and a free surface above the inlet is maintained. During the experiments the pulse rate of the pump is kept high so that it would be effectively dissipated.

The swirl velocity component is imparted to the jet in the rotating chamber unit. The settling chamber (top part) is composed of a hollow inner perforated cylinder, having a conical end at the bottom, and a co-axial outer cylinder connected to a smooth converging nozzle shape (having a fifth-order polynomial profile) at the bottom. Swirl is imparted to the flow as it passes between these two cylinders. Though each of the two cylinders can be rotated independently, in the experiments reported here, only the outer cylinder (including the contraction nozzle) is rotated. Digital control motors, mounted on a different base and connected to the rotating chamber by an elastic belt, provide this rotation very precisely ($\pm 0.08\%$) and allow the swirl to be gradually changed ($0.05\%\ s^{-1}$ for rotation) during experiments. The vibration amplitude of the rotating chamber was found to be 0.15% of the jet exit diameter.

Water is supplied through three pipes symmetrically positioned on the top of the inner cylinder. During filling, the water flows through the network of holes into the gap separating the inner and outer cylinders. It then flows downwards through a perforated ring (attached to the inner cylinder) before entering the nozzle part of the chamber. The exit diameter is 19.6 mm whereas the outer diameter of the attached

cylindrical test section is 226 mm and its height is 470 mm. The resulting ratio of diameters ($\approx$11.5) is found to be sufficient to minimize the effect of confinement. Furthermore, to avoid any return flow, screens are placed at the bottom of the tank, upstream of the four exit pipes.

The temperature difference between the jet and the ambient fluid is the third independent parameter. During the experiments, the temperature of the ambient water in the cylindrical test section is maintained in the range of 296 ± 0.5 K using the room air-conditioning system. To control the temperature of the jet, the supplied water is passed through a helical-coil heat exchanger immersed in a circulating water bath with a controlled temperature. The circulating bath (HAAKE) can provide a wide temperature range (263–373 K) and a precise temperature control ($\pm$0.1)K. A T-type thermocouple, positioned at the entrance to one of the three water-supplying pipes (thermocouple 1), is used to regulate the jet temperature at the nozzle exit. Two additional thermocouples positioned at the inner top part of the test section (thermocouple 2) and at its bottom exit (thermocouple 3), are used to monitor the ambient temperature during the experiments. A mobile thermocouple is used to measure the temperature along the centreline. The tube connecting the bath and the settling chamber as well as the large tank are thermally insulated by foam, except for two small windows (5×7 mm, and 7×7 mm) necessary for the laser sheet and the camera view, respectively.

The difference between the readings of thermocouples 1 and 2 is identified as the temperature difference between the swirling jet and the ambient fluid. Whenever a change in the temperature difference between the two readings was noticed, it was compensated manually by adjusting the bath temperature and consequently fixing the temperature of the jet. Thus, although the room temperature could have varied a little (less than 1 K) during the entire period of experiments the difference between the jet and the ambient fluid at the exit cross-section was less than 0.1 K. Furthermore, to ensure that the temperature variation of the ambient fluid is less than $\pm$0.5 K, the duration of each experiment was limited. For the extreme case reported here, for which the jet was 5 K hotter than the ambient fluid, the experimental duration was 5 min. The minor variation of the room temperature has little effect on the value of the fluid viscosity and the corresponding Reynolds number.

As there is a temperature difference between the position of thermocouple 1 and the mid-point of the jet exit plane, the mobile thermocouple is placed in the latter position. The difference between its reading and that of thermocouple 2 is measured for several Reynolds numbers (while the outer cylinder is kept stationary) and calibrated against the difference between thermocouples 2 and 1. After the calibration procedure is finished, the mobile thermocouple is removed. Assuming the effect of swirl on the temperature at the mid-point of the jet exit plane to be negligible, the temperature difference between the jet and its surroundings could then be directly obtained during the experiments.

For reasons to be explained in § 4.3, several sets of measurements were repeated in another apparatus, similar to the one used by BCH. For these sets of measurements, the inner cylinder was replaced by a cylindrical honeycomb, having a diameter of 45 mm and height of 50 mm, placed adjacent to the top of the converging nozzle and connected to the outer cylinder. Swirl was imparted by rotating the outer cylinder together with the honeycomb. It should be noted that relative to the present apparatus, the outer cylinder of BCH is fixed and the dimensions of their honeycomb are about four times larger. The two setups used in the current study are respectively referred to as IC (inner cylinder) and IH (inner honeycomb).

3.2. *Experimental measurement techniques*

A particle image velocimetry (PIV) system (Dantec) is utilized to visualize the flow and to measure the instantaneous and mean velocity fields. For this purpose, the water is uniformly seeded with 10–50 micron neutrally buoyant hollow silver-coated glass spheres. The PIV system is operated with a 5 W argon ion CW laser operating at 4–5 W. For measurements of the axial and radial velocities, the mid-plane is illuminated by a vertical light sheet which is generated by deflecting an argon-ion laser beam on a rotating polygon mirror. The illuminated plane is imaged from the side on a double-frame 768×480 CCD camera. A pair of two consecutive images, acquired with a controlled time delay is subsequently processed with a cross-correlation algorithm to produce vector maps of the instantaneous flow field. Each frame is divided into 32×32 pixels interrogation areas with 50% overlap. The mean velocities are computed by averaging 400 instantaneous fields acquired at a range of sampling frequencies between 0.3 and 1.0 Hz. The azimuthal and radial velocities in a given cross-stream plane of the jet are measured by a similar procedure to that described above. In this case, however, the illuminated horizontal plane is viewed from the bottom of the tank using a 45° inclined mirror.

3.3. *Experimental procedure*

To obtain the critical conditions for the onset of VB, the rotation rate was increased (by a computer-controlled motor) from zero in gradually decreasing small steps ($\approx$10% of Ω_C – the critical rotation rate needed for initiating VB), while keeping the flow rate and ΔT constant. As Ω_C is approached, the rotation rate was increased by smaller steps of $2\% - 5\%$ of Ω_C (depending on the Reynolds number, the definition of which is based on the average axial velocity at the nozzle exit and its diameter). To avoid transient effects, a waiting period of $\approx$15 min was allowed after each adjustment.

To experimentally verify the modified criterion for VB, the terms S_{int} and Ri of (2.5) were calculated. To calculate S_{int}, the azimuthal velocity profile as well as the axial velocity at the jet axis, in the plane X_1, sufficiently upstream of the stagnation point, were measured. To avoid the influence of the stagnation point on the upstream measured velocities, the procedure employed by BCH was adopted here. Accordingly, the measured velocities in X_1 (4 mm downstream of the jet exit plane) were obtained at a rotation rate of $\Omega = 0.97\Omega_C$.

Examples of axial velocity profiles obtained for different swirl ratios at $Re = 500$ and $\Delta T = 0$ K, are shown in figure 3(*a*), where R is the nozzle exit radius. Positive and negative values of r respectively correspond to the two opposite sides of the measurement plane where $\theta = 0°$ and 180°. For the case without swirl, the central part of the profile has a wake-like shape resulting from our apparatus having an inner conical (IC) part. As the swirl is increased, the wake profile is first replaced by a plateau and then by a jet-like profile at swirl ratios close to the onset of VB. It should be noted that the resulting standard deviation of the flow rate is about 1% of its average value.

The azimuthal velocity profiles measured every 15° along the azimuthal coordinate at $\Omega/\Omega_C = 0.97$ are shown in figure 3(*b*). The profiles were obtained by Lagrangian interpolation from the cross-stream PIV vector map. As can be deduced, the flow at this upstream position is quite axisymmetric. The integral in S_{int} was calculated for each of the profiles and then averaged.

To calculate Ri, the distance H between the plane containing the stagnation point and X_1 was measured. For given Reynolds number and temperature difference, the rotation rate was increased gradually towards its critical value Ω_C (known from

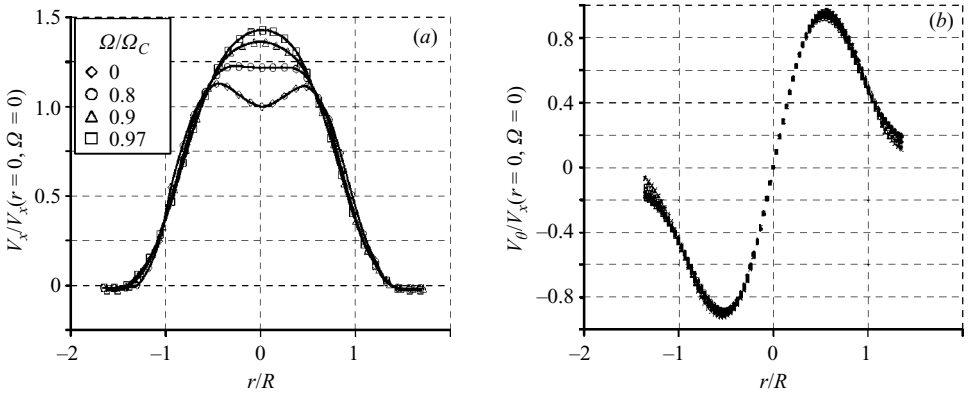

FIGURE 3. Velocity profiles measured at $x = X_1 = 4$ mm, $Re = 500$, $Ri = 0$ and normalized by the centreline axial velocity of the corresponding non-swirling jet. (*a*) Axial velocity profiles at several swirl ratios and (*b*) azimuthal velocity profiles measured every 15° along the azimuthal coordinate at $S_{int} = 0.51$.

previous measurements). An example of the instantaneous flow field in the vertical mid-plane at such conditions is shown in figure 4(*a*). It then was few seconds before the stagnation point first appeared (figure 4*b*). H is defined as the distance between X_1 and the cross-section plane where the stagnation point is first observed. This choice of definition was necessary because after its initiation, the stagnation point moved upstream, affecting the velocity field, measured previously at $\Omega = 0.97\Omega_C$. As the location of the birth of the stagnation point varies from one experiment to another we have measured its value in twenty experiments carried out under the same conditions ($Re = 246$, $Ri = -0.21$, $S_{int} = 0.78$). The resulting standard deviation of H was found to be 3.6% of its average value.

Prior to the onset of breakdown the flow can be considered as steady. However, after its initiation, the stagnation point moves upstream implying that the flow has not reached a steady state. Thus, the condition of steadiness necessary to apply the criterion (2.5) may not be fully fulfilled. To find the relative importance of the unsteadiness of the flow, we have compared the ratio between $(\partial V_x/\partial t)$ and $(\partial V_x^2/\partial x)$ at different times past the initiation of the VB and at various streamwise positions along the centreline and upstream of the stagnation point. The average value of 40 ratios (obtained at various streamwise positions and at several times) is found to be ≈ 0.07 for an isothermal jet at $Re = 246$, and ≈ 0.09 for a colder jet for the same Reynolds number and $Ri = 0.12$, justifying the assumption of steadiness as a first approximation.

4. Results and discussion

4.1. *Verification of the simple criterion for the onset of VB*

The theoretically obtained necessary condition for vortex breakdown (2.5) is compared with experimental results in figure 5 for a range of $-2.5 \leqslant \Delta T[K] \leqslant 5$ and for two Reynolds numbers of 246 and 500. Open symbols and filled symbols correspond to the IC and IH experimental setups, respectively. In the plane of S_{int} vs. Ri the criterion is a straight line. Good agreement between the modified theoretical model and the experimental data is obtained. It is also evident that the onset of vortex breakdown for all cases considered is slightly above the inviscid theoretical criterion,

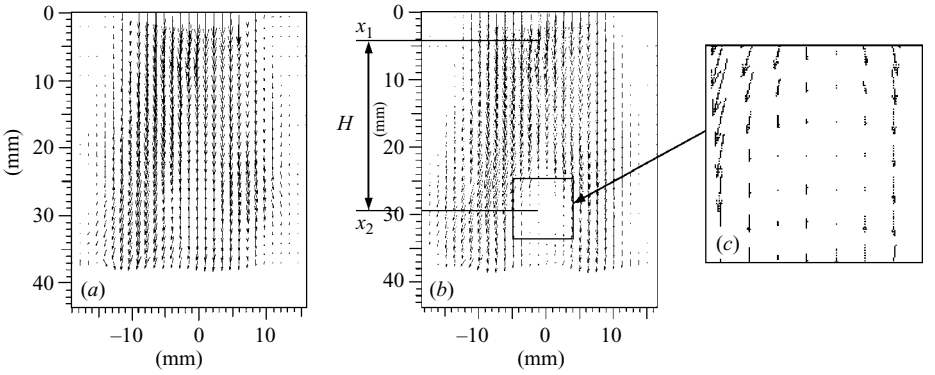

FIGURE 4. Definition of H. Instantaneous flow field in the vertical mid-plane at critical conditions; jet flows from top to bottom; $Re = 246$, $Ri = 0$, and $S_{int} = 0.53$. (*a*) $t = 0$, (*b*) initiation of a stagnation point at $t = 2$ s, (*c*) closeup of the stagnation point region.

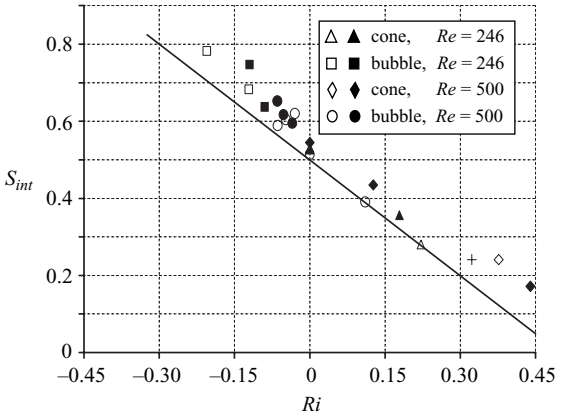

FIGURE 5. Experimental verification of the breakdown criterion. Open and filled symbols correspond to the IC and IH apparatus, respectively. The solid line shows the theoretical criterion.

probably due to viscous effects. As pointed out by BCH for an isothermal jet, the discrepancy becomes larger at smaller Reynolds numbers. In this respect, it should be noted that the results presented in their figure 12, correspond to relatively higher Reynolds numbers (450–850). Furthermore, as S_{int} is the square of their critical swirl number (S_i), a relative error of 10% in S_i would appear as an error of $\approx$21% in S_{int}. Another source of error is the temperature variation of the jet along the downstream direction. For $\Delta T < 0$ this effect was found to be negligible. However, for warmer jets, the axial temperature gradient becomes more significant with increasing ΔT. For the most extreme case presented in figure 5 for the IC configuration, the relative error is about 23% over the distance H. In this case, when the axial average value of ΔT is used, the corresponding point moves towards the theoretical criterion (its new position is indicated by the plus symbol). The vertical temperature gradient in the ambient fluid in most cases is nearly zero and can reach a maximum value of $0.02\,\mathrm{K\,cm^{-1}}$ for the case of the warmest jet. This gradient can be represented by the Rayleigh number ($Ra = g\beta\Delta T H^3/(\nu k)$, where k is the thermal diffusivity) indicating the importance of thermal convection effects in the tank. Although Ra can be large

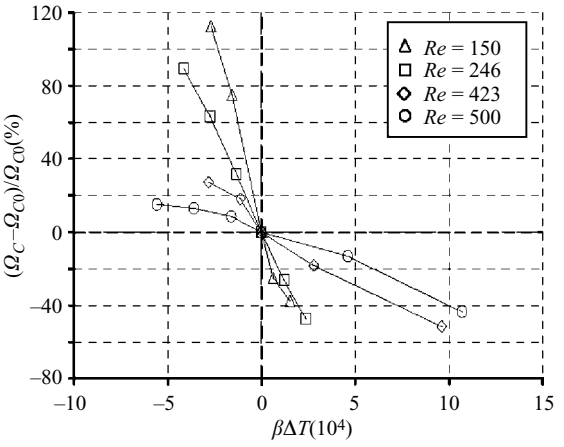

FIGURE 6. Delaying/advancing the onset of vortex breakdown by thermal effects in the range $150 \leqslant Re \leqslant 500$, IC apparatus. $\Omega_{C0} \equiv \Omega_C$ ($\Delta T = 0$).

($\propto H^3$) our PIV measurements at the vicinity of the jet show zero velocity of the ambient fluid.

A further validation of the VB criterion is carried out for a specific case in which the jet is hotter than the ambient fluid and the end position of the stagnation point remains sufficiently far downstream from the jet exit plane (figure 7*d*). The criterion is checked at four streamwise positions (4, 6, 8 and 10 mm from the jet exit) corresponding to four different choices of X_1. These positions are indicated in figure 7(*d*) by the black dots. As we are not able to simultaneously measure the vector map in the (r, θ) plane (to obtain the azimuthal profiles) and the map in the vertical plane (to obtain $V_x(r = 0)$ and H), we have used five different sets of measurements of the vertical plane and three sets of measurements of the cross-section plane for each of the four streamwise positions. The average value of VB_{crit} is 0.51 for all 60 cases with a standard deviation of $\approx$0.05. However, as the results associated with the four cross-sectional maps which were measured successively within 25 min, can be grouped together, the number of independent cases can be reduced to 15. The resulting averaged standard deviation of VB_{crit} obtained in this case is 0.0147.

A quantitative measure of VB suppression and enhancement is presented in figure 6. This is done by measuring the reduction percentage of the critical dimensional swirl (Ω_C), relative to its value at $\Delta T = 0$ (labelled Ω_{C0}). Colder jets (relative to the ambient fluid) would cause the suppression of VB whereas warmer jets would cause its enhancement. For all Reynolds numbers considered, the amount of suppression increases monotonically as ΔT is decreased. (Here β is used to normalize the temperature difference.) For lower Reynolds numbers buoyancy becomes dominant and therefore the suppression is more effective. As the temperature difference between the jet and its surroundings is decreased higher rotation rates are needed to initiate VB.

4.2. *Parameters determining the configuration of VB*

The temperature difference between the swirling jet and ambient fluid affects the final form of VB, i.e. the shape of the recirculation zone. In figure 7(*a–d*) this effect is demonstrated for a fixed Reynolds number of $Re = 246$. At $Ri = -0.03$ (colder jet) the final configuration has a bubble shape (figure 7*a*), i.e. the relative fast flow enclosing the stagnation zone (including the stagnation point and its downstream low-velocity recirculation region) first expands radially and then, beyond a certain

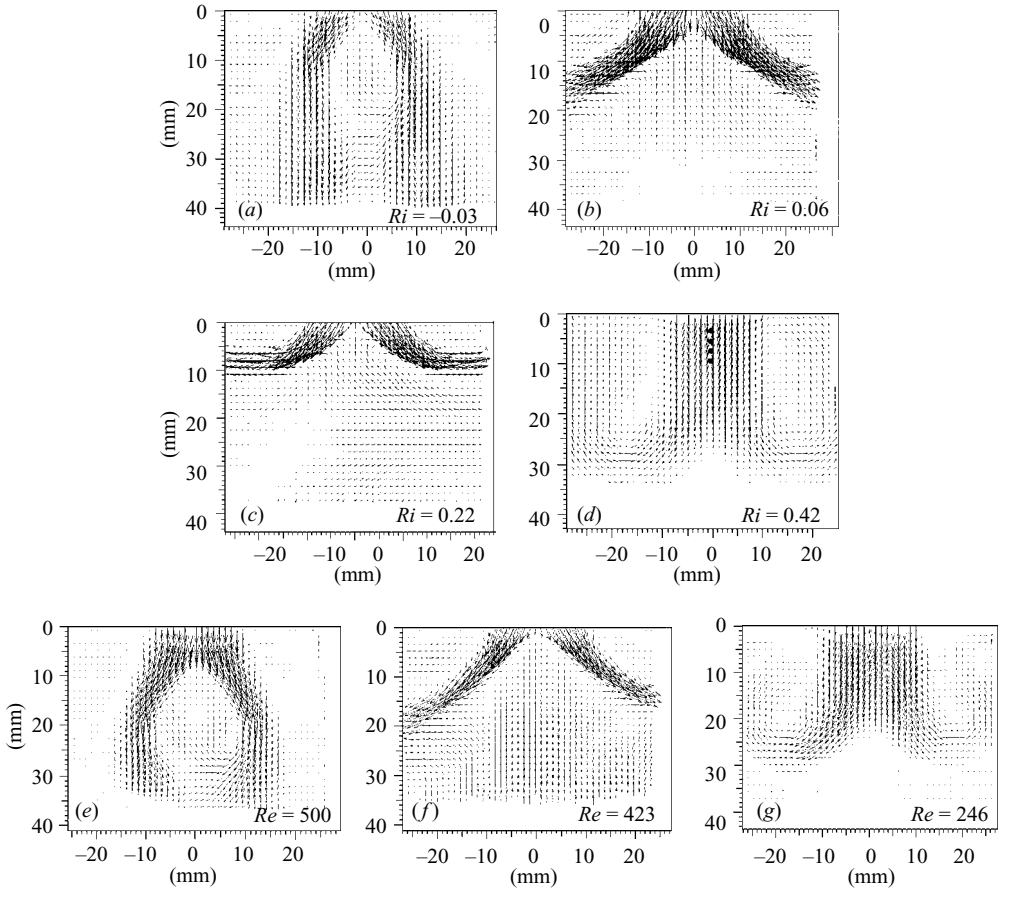

FIGURE 7. Effect of Ri (*a–d*, $Re = 246$) and Re (*e–g*, $\Delta T = 1.1\,\mathrm{K}$) on the VB configuration at the vertical mid-plane, IC apparatus (jet flows from top to bottom and shown by vector maps averaged over 100 s). (*a*) $S_{int} = 0.64$, (*b*) $S_{int} = 0.48$, (*c*) $S_{int} = 0.28$, (*d*) $S_{int} = 0.13$, (*e*) $S_{int} = 0.47$, (*f*) $S_{int} = 0.36$, (*g*) $S_{int} = 0.15$.

downstream distance, contracts. As the jet temperature (and its associated Richardson number, Ri) are increased VB occurs at a lower swirl and the bubble size increases until it transforms into an open cone (figure 7*b*). With a further increase of Ri a wide open cone is formed (figure 7*c*) and then, for a larger temperature gradient ($Ri = 0.42$), a downstream movement of the stagnation point takes place (figure 7*d*). Reducing Re while keeping ΔT constant, has qualitatively the same effect as increasing the temperature of the jet, i.e. transforming the bubble (figure 7*e*) into a $\approx 90^\circ$ open cone (figure 7*f*) and then to a wide open cone which occurs further downstream (figure 7*g*).

The above results suggest the existence of two separate zones in the Re–Ri map where cones and bubbles may be observed. Therefore, for seven Reynolds numbers we have searched for the ΔT associated with a boundary between these two configurations. These boundary points are shown in figure 8 by the open circles. To the right (left) of this boundary only cones (bubbles) have been observed (without mixed states). For a given Reynolds number, the boundary point was not sensitive to the approaching direction, i.e. increasing or decreasing Ri, and therefore no indication of hysteresis was observed. At one such boundary point, enclosed by the dotted circle (in figure 8), we have examined the long time dynamics of the vortex structure

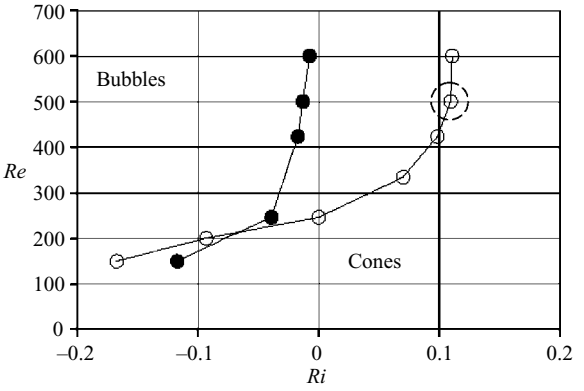

FIGURE 8. The boundary between cone and bubble configurations. Open and filled circles correspond to the IC and IH experimental setups, respectively.

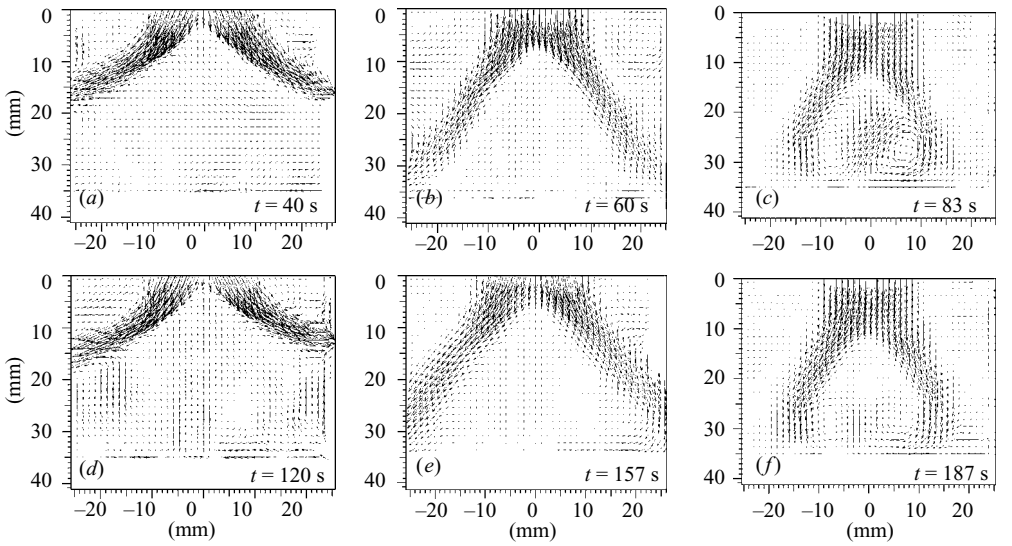

FIGURE 9. Periodic behaviour of VB configuration shown in the vertical mid-plane, jet flows from top to bottom and shown by instantaneous vector maps. $Re = 500$, $Ri = 0.11$, $S_{int} = 0.39$, IC apparatus.

(figure 9). The vortex configuration displays a quasi-periodic behaviour: the opening angle of the cone (figure 9*a*) is first decreased (figure 9*b*) and then the vortex shape becomes that of a bubble (figure 9*c*) before increasing again and returning to its initial form (figure 9*d*) and repeating the previous cycle (although with longer time intervals). At least three such cycles have been observed before the vortex reaches its final configuration. It should be noted that regular oscillations of the cone opening angle have been reported by BCH but the cone even in its closest form was still different from a bubble.

4.3. *Effect of the upstream velocity field*

The effect of ΔT on the form of VB was reported by BCH who pointed out that the selection of breakdown state is extremely sensitive to small temperature

inhomogeneities present in the apparatus and that a small amount of positive and negative $\Delta T = 0.1\,\mathrm{K}$ promotes a cone and bubble, respectively. On the other hand, unlike the present results, in their experiments bubbles and cones were found to coexist (above the threshold swirl) at the same Reynolds number. To resolve this issue a second set of measurements was carried out in another apparatus (IH), similar to the one used by BCH, in which the inner cylinder was replaced by a cylindrical honeycomb. For this apparatus, the ΔT identified with the boundary separating the two flow configurations does indeed not depend on Re and is slightly below zero. When the results for both setups are plotted on a Re vs. Ri map (figure 8), the two curves, although being different, do have similar trends. For $Re < 300$ the boundary position varies significantly with Ri whereas for $Re > 450$ it approaches a constant value of Ri. The constant value, however, depends on the apparatus. As was already shown in figure 5, the experimental verification of the breakdown criterion is valid for both experimental setups.

The difference between the results (presented in figure 8) associated with the two facilities is probably related to the upstream velocity field. Without any swirl the axial velocity profile of the IC apparatus is that of a wake whereas that of the IH setup has a top-hat shape. With increasing swirl their initial shapes become more similar although they are still different. Mean velocity profiles (not shown here), measured along the axial direction at several Reynolds numbers, indicate that viscous effects are more pronounced in the IC apparatus (for the lower part of the Reynolds number range investigated). In this respect it should be pointed out that BCH have reported a strong effect of the nozzle diameter. For a larger nozzle diameter they have observed the cone mainly for large $Re > 600$ and the bubble for $Re < 800$. With a smaller nozzle the situation was somewhat reversed. This together with the present results suggest that differences in the velocity profiles (in addition to buoyancy effects) can be responsible for the selection of the breakdown state.

5. Conclusions

The simple criterion for the onset of vortex breakdown proposed by BCH is modified to include buoyancy effects. The modified criterion is shown to predict the critical swirl number for the onset of VB as function of the Richardson number. Consequently, suppression (enhancement) of VB by buoyancy effects is demonstrated. The VB configuration as a function of the Reynolds and Richarson numbers is mapped. As the Reynolds number is increased the transition between cone and bubble configurations occurs at lower values of Ri. For sufficiently high Reynolds numbers ($Re > 300$), the boundary between cones and bubbles seems to be independent of the Reynolds number. At the boundary between the two configurations, the shape of vortex structure displays a quasi-periodic behaviour: the cone changes into a bubble, then back to a cone and to a bubble again. Finally, the important effect of the upstream velocity field on the critical rotation rate for the onset of VB and its configuration is exhibited.

Special thanks go to Alexander Svizher for fruitful and stimulating discussions. The technical assistance of Efim Shulman, Oleg Kan and Amos Beer are gratefully acknowledged. The authors thank Joseph Tanny and Jimmy Philip for their careful reading of the manuscript and valuable comments.

REFERENCES

Arkadyev, A., Bar-Yoseph, P., Solan, A. & Roesner, K. 1993 Thermal effects on axisymmetric vortex breakdown in a spherical gap. *Phys. Fluids* A **5**, 1211.

Billant, P., Chomaz, J. M. & Huerre, P. 1998 Experimental study of vortex breakdown in swirling jets. *J. Fluid Mech.* **376**, 183 (referred to herein as BCH).

Escudier, M. P. & Keller, J. J. 1983 Vortex breakdown: a two-stage transition. *Aerodynamics of Vortical Flows in Three Dimensions. AGARD CP*-342 (ref 25).

Gallaire, F. & Chomaz, J. M. 2003*a* Instability mechanisms in swirling flows. *Phys. Fluids* **15**, 2622.

Gallaire, F. & Chomaz, J. M. 2003*b* Mode selection on in swirling jet experiments: a linear stability analysis. *J. Fluid Mech.* **494**, 223.

Gallaire, F., Rott, S. & Chomaz, J. M. 2004 Experimental study of a free and forced swirling jet. *Phys. Fluids* **16**, 2907.

Gallaire, F., Ruith, M., Meiburg, E., Chomaz, J. M. & Huerre, P. 2006 Spiral vortex breakdown as a global mode. *J. Fluid Mech.* **549**, 71.

Herrada, M. A. & Shtern, V. 2003*a* Control of vortex breakdown by temperature gradient. *Phys. Fluids* **15**, 3468.

Herrada, M. A. & Shtern, V. 2003*b* Vortex breakdown control by adding near-axis swirl and temperature gradients. *Phys. Rev.* E **68**, 041202–1.

Ivanic, T., Foucault, E. & Pecheux, J. 2003 Dynamics of swirling jet flows. *Exps. Fluids* **35**, 317.

Kim, W. N. & Hyun, J. M. 1997 Convective heat transfer in a cylinder with a rotating lid under stable stratification. *Intl J. Heat Fluid Flow* **18**, 384.

Lee, C. H. & Hyun, J. M. 1999 Flow of a stratified fluid in a cylinder with a rotating lid. *Intl J. Heat Fluid Flow* **20**, 26.

Liang, H. & Maxworthy, T. 2005 An experimental investigation of swirling jets. *J. Fluid Mech.* **525**, 115.

Lim, D. W. & Redekopp, L. G. 1998 Absolute instability conditions for variable density, swirling jet flows. *Eur. J. Mech.* B/*Fluids* **17**, 165.

Loiseleux, T. & Chomaz, J. M. 2002 Breaking of rotational symmetry in a swirling jet experiment. *Phys. Fluids* **15**, 511.

Loiseleux, T., Delbende, I. & Huerre, P. 2000 Absolute and convective instabilities of a swirling jet/wake shear layer. *Phys. Fluids* **12**, 375.

Lugt, H. J. & Abboud, M. 1987 Axisymmetrical vortex breakdown with and without temperature effects in a container with a rotating lid. *J. Fluid Mech.* **179**, 179.

Martin, J. A & Meiburg, E. 1994 On the stability of swirling jet shear layer. *Phys. Fluids* **6**, 424.

Ruith, M. R., Chen, P., Meiburg, E. & Maxworthy, T. 2003 Three-dimensional vortex breakdown in swirling jets and wakes: direct numerical simulation. *J. Fluid Mech.* **486**, 331.

Shtern, V., Hussain, F. & Herrada, M. 2000 New features of swirling jets. *Phys. Fluids* **12**, 2868.

Sun, D. J., Hu, G. H., Gao, Z. & Yin, X. Y. 2002 Stability and temporal evolution of a swirling jet with centrifugal unstable azimuthal velocity. *Phys. Fluids* **14**, 4081.

Wang, S. & Rusak, Z. 1977 The dynamics of a swirling flow in a pipe and transition to axisymmetric vortex breakdown. *J. Fluid Mech.* **340**, 177.